A Computer-Aided System for Melt Quality and Shrinkage Propensity Evaluation Based on the Solidification Process of Ductile Iron

P. Larrañaga, J. M. Gutiérrez, A. Loizaga, J. Sertucha, R. Suárez

Engineering and Foundry Dept., Azterlan Metallurgical Center, Durango (Bizkaia), Spain.

ABSTRACT

The present work develops a new method for pre-evaluating melt quality of ductile irons and for predicting their metallurgical behavior during the solidification step. Based on the characterization of the liquid-solid transition using the cooling curves and database techniques, this study provides a new effective approach to predict the nucleation ability of the metal and its shrinkage formation tendency. Both factors are considered as critical parameters in order to guarantee the effective manufacturing of sound castings and increase the productivity. Two specific parameters have been defined for this purpose: N (nodule count prediction factor) and k (shrinkage formation tendency factor). A thermal analysis database has been set up by analyzing castings of an extended variety of ductile irons manufactured under fixed production conditions. This database contains more than 600 records obtained from experimental cooling curves, the results of metallographic studies (graphite morphology characterization), the chemical composition of the alloy and X-ray inspections for evaluating the appearance of contraction defects in specific samples. It is found that necessary feeding requirements related to riser design and the contraction defects appearance are strongly correlated to the shape of the cooling curves and the corresponding N and k factors. Therefore, it is possible to predict the metallurgical behavior of alloys by analyzing their solidification before casting. The aim of the present work is to introduce the procedure for evaluating the N and k factors and to describe their effectiveness when compared to the information from the database.

INTRODUCTION

Although many improvements have been made regarding ductile iron manufacturing processes, unsound castings are still produced under normal production conditions. It is known that different metallurgical behaviors, such as nodule count, shrinkage appearance and carbide formation, can be obtained using similar chemical alloy compositions, inoculation procedures and sand molding processes. These experimental variations have been generally attributed to important differences concerning solidification processes of the liquid iron that originate as a consequence of many processing factors such as the metallic charge materials, the melting and the Mg treatment methodologies[1-3].

Due to lack of knowledge as to how all those factors influence SG iron solidification processes, several papers have been published containing different methods for this purpose.[2, 4-8] In this context, thermal analysis concerning the cooling curves have been one of the most used techniques for investigating the solidification processes of ductile irons. Although this technique has been used for chemical determinations (carbon, silicon and carbon equivalent contents),[9-10] its principal advantage consists in the fact it provides a way to analyse the different steps of the liquid-solid transformation and to establish relationships between the cooling curve parameters and the metallurgical characteristics of the alloy[11-14]. According to this, an extensive number of technical works concerning the eutectic and eutectoid transformations in graphitic irons have been published and, as a result of them, several mathematical models and data bases have been developed including final prediction systems.[2, 4-5 ,15-21] Thus, thermal analysis has been employed for obtaining information regarding the inoculation efficacy[16,22-23], mechanical properties and hardness predictions[17,21,24], graphite morphology[2,5,15,18], latent heat calculations[15,25-26], shrinkage tendency[6,8,11,27-28] and the graphite nucleation potential during the solidification process[2,29-33].

The resulting information can be stored into a data base which may be used to control the real manufacturing process at foundries and avoid the appearance of metallurgical defects in cast parts. Research results show that variations in processing factors also influence the shape and characteristics of the cooling curves. This fact has served as an incentive to develop new studies and systems in order to extend the thermal characterization to the subsequent steps of ductile iron manufacturing processes[34-36]. However, such results should be considered as exclusive parameters in each foundry, as they can only be safely used in well-controlled processes[37].

This work provides a new solidification model based on cooling curves for evaluating melt quality as a function of the graphite formation, nodule count and the contraction-expansion balance in iron samples analyzed in plant before mold pouring. An additional novelty lies in the fact that both austenite and graphite formation are characterized and related to

different cooling curves and to the metallurgical behavior of castings. Consequently, it has been necessary to develop new thermal analysis tests in order to determine carbon, silicon and active magnesium dissolved in Mg-treated irons and compare these results with information obtained from methods normally used in foundries[38]. In this way, a shrinkage formation prediction through cooling curves analysis can be considered essential to minimize engineers modifications based on their experience and trial and error tests[39]. The resulting correlations will be discussed along this article.

THEORY OF SOLIDIFICATION BASED ON COOLING CURVES

As illustrated in Figure 1, the liquid-solid transformation of graphitic irons observed on cooling curves presents characteristic features. The solidification process occurs in three successive stages:

- While the cooling rate is considered to be constant until the liquidus temperature is reached, a slope change is observed when the first austenite crystals and/or graphite nodules are formed.
- The second stage corresponds to the bulk liquid-solid transformation, during which both austenite and graphite crystals form and progressively grow. Austenite can appear as metallic shells surrounding the graphite nodules and/or as free dendrites, this is the so-called eutectic plateau.
- During the final solidification step, grain boundaries are generated from residual liquid into the solid network.
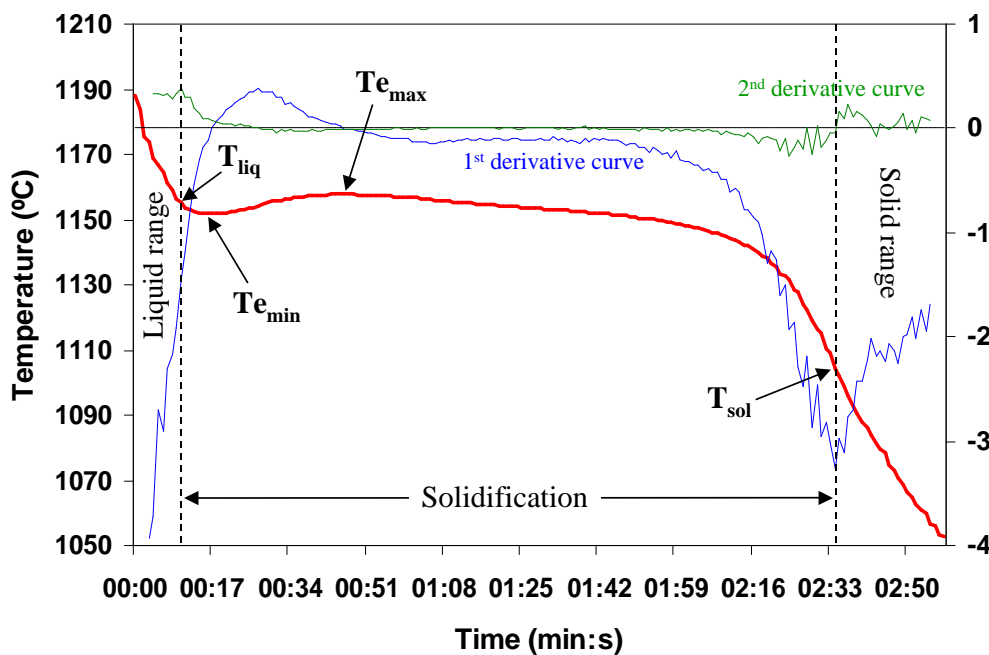

Figure 1. Solidification curve and thermal parameters used in the present work.

Figure 1 shows the critical temperatures defined in order to characterize the solidification curves: liquidus temperature (T_{liq}), minimum eutectic temperature (Te_{min}), maximum eutectic temperature (Te_{max}) and solidus temperature (T_{sol}). These parameters are calculated in all cases using the first and second derivative curves. In addition, the recalescence Rc is given as $Te_{max} - Te_{min}$.

HEAT BALANCE DURING PHASE TRANSFORMATION

The evolution of the mass of austenite and of graphite during solidification will be evaluated following a simple procedure using the cooling curve recorded by standard thermal analysis (TA). The overall heat flux out off a TA standard sample may be written as a first approximation as the sum of the loss of energy of the material due to the decrease in temperature and the latent heat release due to austenite (λ_γ) and graphite (λ_G) precipitation:

$$\Phi_{Sample} = -\left[m_{Sample} \cdot c_p \cdot \frac{dT_{Sample}}{dt} + \lambda_\gamma \cdot \frac{dm_\gamma}{dt} + \lambda_G \cdot \frac{dm_G}{dt} \right]$$

Equation 1

where Φ_{Sample} is the total heat flux extracted from the sample, $m_{Sample} \cdot c_P \cdot \dfrac{dT_{Sample}}{dt}$ is the term due to cooling of the sample, $\lambda_\gamma \cdot \dfrac{dm_\gamma}{dt}$ is the latent heat release due to austenite solidification and $\lambda_G \cdot \dfrac{dm_G}{dt}$ is latent heat release related to graphite precipitation. The range of temperatures where the liquid-solid transformation takes place in ductile iron is narrow enough in order to consider the specific heat (c_p) as a constant, and it will be assumed equal for liquid and solid.

In order to estimate the energy associated to solidification, the experimental cooling curves are compared to a reference cooling curve obtained assuming that the sample does not undergo any phase transformation (Figure 2). In this reference case, the overall heat flux ($\Phi_{Reference}$) out off the sample cup is written as follows:

$$\Phi_{Reference} = -\left[m_{Sample} \cdot c_p \cdot \frac{dT_{Reference}}{dt} \right] \qquad \text{Equation 2}$$
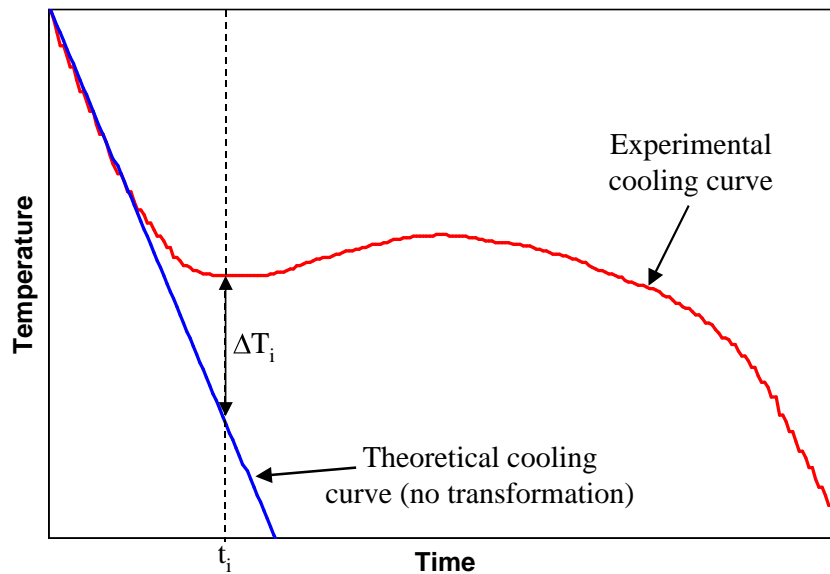
Figure 2. Comparison between an experimental and the reference (with no transformation) cooling curves.

In Figure 2 is defined the temperature difference $\Delta T_i = (T_{Sample_i} - T_{Reference_i})$ between the measured sample temperature and the calculated reference temperature. The subscript i indicates that the data are discretized in time, with index "i" referring to time step i. The change in ΔT_i is associated to the instantaneous latent heat release only. Combining equations 1 and 2 gives:

$$m_{Sample} \cdot c_p \cdot \delta\Delta T_i = \lambda_\gamma \cdot \delta m_{\gamma_i} + \lambda_G \cdot \delta m_{G_i} \qquad \text{Equation 3}$$

where δm_{γ_i} and δm_{G_i} are the instantaneous change in mass of austenite and graphite respectively.

Integrating equation 3 thus relates the experimental cooling curves to the total mass of austenite and graphite depositing during solidification. On the other hand, the final values of austenite and graphite formed during solidification of the sample (m_γ and m_G) depend on the chemical composition of the melt. The total carbon and silicon contents of the melt, respectively %C and %Si expressed in wt. %, can be obtained using thermal analysis experiments[9-10]. Further, considering that the amount of carbon dissolved in austenite is conveniently evaluated as 2.03-0.20·%Si, the total amount of graphite formed at the end of solidification is then calculated as follows[37]:

$$m_G = \frac{m_{Sample}}{100} \cdot \left(\%C_{Total} - \%C_\gamma \right) = \frac{m_{Sample}}{100} \cdot \left[\%C_{Total} - \left(2.03 - 0.20 \cdot \%Si \right) \right] \qquad \text{Equation 4}$$

in which m_{Sample} is the mass of the standard sample that can be obtained from the time of cooling of the metal through a defined range of temperatures. In our case, the 1210-1050ºC range has been selected because the solidification of the sample is guaranteed into it.

The total amount of austenite can then be calculated as the difference between the total mass of the analyzed sample and that corresponding to the graphite precipitated ($m_\gamma = m_{Sample} - m_G$). Because the nearly isothermal eutectic plateau is known to relate to solidification kinetics that is nearly linear in time, it is proposed to write that such a simple evolution applies to austenite precipitation. The instantaneous discretized change in austenite mass is thus assumed to be given as:

$$\delta m_{\gamma_o} = \frac{m_\gamma}{t_{solidus} - t_{liquidus}} \cdot \delta t_i \qquad \text{Equation 5}$$

where δm_{γ_o} is thus the amount of austenite that should precipitate during time step i in order to obtain the total mass of austenite in the sample (m_γ) at the end of an ideal solidification process with linear solidification kinetics. Analysis of the experimental cooling curves shows however that there are time steps where the actual heat flux available for the phase change (given by equation 3) is lower than the necessary one for crystallizing the quantity of austenite expected from equation 5. In those cases, all the available latent heat release is assumed to lead to austenite deposition. In all practicality, successive corrections are needed in the theoretical value of austenite for each of the time periods when ΔT_i is lower than necessary. These corrections are successively added so that after 1 and n time steps one has:

$$\delta m_{\gamma_1} = \delta m_{\gamma_o} + \frac{\left(\delta m_{\gamma_o} - \frac{m_{Sample} \cdot c_P \cdot \delta \Delta T_1}{\lambda_\gamma} \right)}{\Delta t_o} \qquad \text{Equation 6}$$

$$\delta m_{\gamma_n} = \delta m_{\gamma_o} + \sum_{i=1}^{n} \frac{\left(\delta m_{\gamma_{i-1}} - \frac{m_{Sample} \cdot c_P \cdot \delta \Delta T_i}{\lambda_\gamma} \right)}{\Delta t_{i-1}} \qquad \text{Equation 7}$$

where Δt_i is the length of time on which the deficit of latent heat release is dispatched. After scanning of the whole cooling curve to determine the successive values of δm_{γ_i} and δm_{γ_n}, the deficit in latent heat release is progressively redistributed in a uniform way as described by Figure 3.
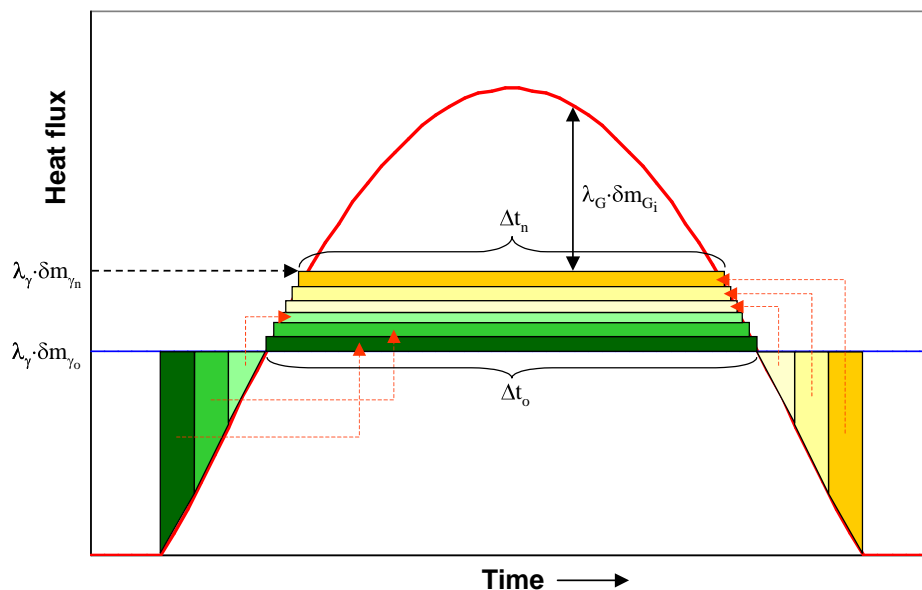

Figure 3. Heat flux evolution in time during the solidification range (austenite and graphite formation areas).

From this, the latent heat release possibly available for graphite precipitation is finally deduced according to equation 8.

$$\delta m_{G_i} = \frac{m_{Sample} \cdot c_p \cdot \delta \Delta T_i - \lambda_\gamma \cdot \delta m_{\gamma_n}}{\lambda_G}$$

Equation 8

CONTRACTION-EXPANSION BALANCE

In the solidification process an important change of volume due to the variation of density between the liquid and the solid phases can occur. This phenomenon is the result of graphite (expansion) and austenite (contraction) crystallization from the liquid and their subsequent growth from the melt. Thus, as the amount of austenite and graphite formed at each period of time (δm_{γ_n} and δm_{G_i}) can be determined using the experimental cooling curves, it is possible to obtain a contraction-expansion balance. The change of volume between two successive time steps due to the formation of austenite and graphite can be calculated as follows:

$$\Delta V_i = V_i - V_{i-1} = \frac{\delta m_{\gamma_n}}{\rho_\gamma} + \frac{\delta m_{G_i}}{\rho_G} + \frac{\delta m_{Liquid_i}}{\rho_{Liquid}}$$

Equation 9

where ρ_γ, ρ_G and ρ_{Liquid} are the densities of austenite, graphite and liquid, respectively. Also, a mass balance gives:

$$\delta m_{Liquid_i} = -\delta m_{\gamma_n} - \delta m_{G_i}$$

Equation 10

Equation 9 may thus be written as:

$$\Delta V_i = \delta m_{\gamma_n} \cdot \left(\frac{1}{\rho_\gamma} - \frac{1}{\rho_{Liquid}} \right) + \delta m_{G_i} \cdot \left(\frac{1}{\rho_G} - \frac{1}{\rho_{Liquid}} \right)$$

Equation 11

Taking into account that the density of austenite is higher than that of liquid and that both are much higher than the density of graphite, the resulting variation of volume may be either negative or positive. Accordingly, the calculation of the volume changes due to the graphite and austenite formed in different steps of the solidification leads to determine the contraction-expansion balance at each time.

NODULE COUNT

The nodule count (expressed as N) plays an important role in the mechanical properties of ductile irons. Therefore, the estimation of this parameter using a standard sample is considered as very relevant in order to obtain a good indicator for evaluating the melt quality in this type of irons. In the present work, an important dependence between several additional parameters obtained directly from the cooling curve and the final nodule count has been found. The evaluation of these parameters can be consequently used for estimating the nucleation ability of the iron during the solidification range.

Bearing this in mind, a wide range of nodule count values has been obtained via metallographic analysis from all experimental tests using inoculated and non inoculated samples. Then, they have been related to the main characteristics of the experimental cooling curves expressed with the parameters evaluated from the first and second derivative curves (Figure 1). In addition, a new parameter (G_R) has been defined according to the equation 12 in order to estimate the graphite formation rate during the solidification process.

$$G_R = \sum_i \frac{m_{G_i}}{\Delta t_i}$$

Equation 12

Under those conditions, a mathematical expression to calculate the nodule count has been developed using four experimental parameters according to equation 13.

$$N = A_1 \cdot Te_{min} + A_2 \cdot Rc + A_3 \cdot G_R + A_4 \cdot \left(\frac{dT}{dt} \right)_{Solidus} + A_5$$

Equation 13

In this expression, the $\left(\dfrac{dT}{dt}\right)_{Solidus}$ term corresponds to the maximum cooling rate at the very end of the eutectic transformation (near to the temperature T_{sol}).

MICROSHRINKAGE TENDENCY

Although they are not the unique main causes, metallurgical behavior during solidification and the evolution of the contraction-expansion balance are critical aspects as to shrinkage defects appearance in ductile iron castings. Therefore, a useful indicator to measure the contraction tendency of the melt must be included into the developed computer-aided system for effective melt quality evaluations.

According to the model calculated for the contraction-expansion balance and the formation of graphite and austenite at different moments of solidification, the experimental cooling curves show an initial contraction period close to the liquidus temperature (Figure 4). This small area is a consequence of the formation of primary austenite. When the transformation goes on, an important expansion period occurs due to graphite precipitation and its subsequent growth. Finally, a contraction range is found at the end of the solidification process. In this last area, graphite expansion decreases and a final net contraction occurs. Microshrinkages are normally formed in this period of time due to the impossibility of liquid feeding through the existing solid network.

The obtained contraction-expansion balance and especially the final contraction period strongly depend on the shape of the experimental cooling curve. In order to evaluate this behavior and consequently the tendency of the melt to form microshrinkages, a new parameter has been defined as:

$$k = \frac{t_{Expansion}}{t_{Expansion} + t_{Final-contraction}}$$

Equation 14

where $t_{Expansion}$ and $t_{Final-contraction}$ are the total periods of time for expansion and for final contraction during the solidification process. In this way, the tendency to microshrinkages formation in a specific ductile iron can be turned into a number only from of metallurgical considerations. Thus, the risk of defect formation decreases when the final contraction periods become smaller and, therefore, the resulting value of the k factor approaches 1.
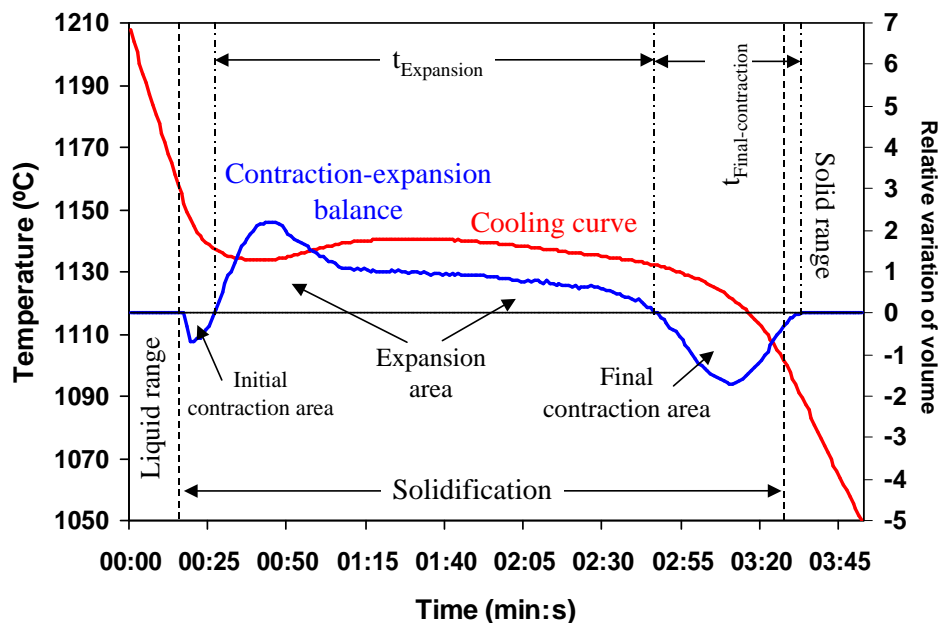

Figure 4. Contraction-expansion balance obtained from an experimental cooling curve.

EXPERIMENTAL

A database has been established including 620 records obtained from different fields: the eutectic transformation parameters of cooling curves, the chemical composition of the alloys, the nodule count estimated using an image analysis software and the tendency to contraction defects appearance calculated from the solidification patterns.

An extensive number of solidification experiments were performed on different ductile iron qualities ranging from EN GJS 400-15U to EN GJS 700-2U. All metal samples used in this work were picked up from the basin area close to the rod stopper in vertically parted automatic molding lines equipped with automatic pouring furnaces. Samples were also collected for later analysis by means of chemical and spectroscopic techniques in all experimental tests in order to compare them with the corresponding thermal analysis results. Table 1 shows the obtained ranges for the most important elements analyzed by chemical techniques and spectroscopy.

Table 1. Chemical Composition Ranges for Melts Used in the Present Work.

C	Si	Mn	P	S	Cu	Mg	Ti
3.50-3.85	2.25-2.80	0.12-0.25	0.020-0.045	0.001-0.006	0.02-1.05	0.025-0.045	0.008-0.026

All liquid metal samples were melted in medium frequency induction furnaces (250 Hz), 7-10 t capacity and 4000-5000 kW power. Two different metallic charges were used in melting area: charge 1 was composed of 40% automotive steel scrap, 10% pig iron and 50% return scrap; charge 2 contained 50% pig iron, 20% automotive steel scrap and 30% return scrap. A commercial recarburizer product and a FeSi alloy were added together with the metallic charges introduced into the furnaces for achieving the desired carbon and silicon contents. After melting, 0.10% of SiC conditioning product was added. Then, carbon and silicon contents were checked by spectroscopic analysis and adjusted to the specified values. Finally, the melt temperature was increased up to 1500ºC (2732F) and its surface skimmed. The liquid metal obtained from furnaces was treated in 1.5-2.0 t capacity ladles with a FeSiMg alloy (5-6% of magnesium content) by means of the tundish cover method. All magnesium treatments were carried out in the 1470-1490ºC (2678-2714F) range. The resulting treated batches were then transferred to the corresponding pressurized pouring devices (8-10 t of capacity).

Thermal analysis tests were recorded in the range of 1210-1050ºC (2210-1922F) in order to characterize the liquid-solid transition in all samples and to determine the critical parameters using a specific thermal analysis software developed in Azterlan (Figure 5). A correct evaluation of thermal parameters requires that the following conditions are fulfilled:
- As the maximum capacity of the pouring cups is 340-350 g, a minimum weight of 320 g must be poured into cups for representative results. The weight of samples should be as constant as possible.
- The components from the sampling cups should not react with the melt.
- Initial temperature of liquid samples has to be high enough for adequate recording of solidification curves.
- A correct inoculation of the melt must be guaranteed.
- Stable conditions at the sampling cups are needed during all data collection process.
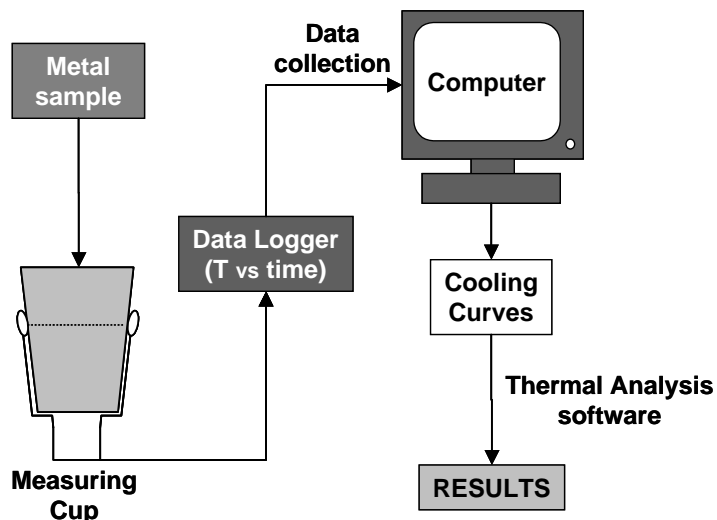
Figure 5. Scheme of the system used for thermal characterizations.

According to these requirements, a considerable amount of metal samples were poured into standard commercial cups with a K-type thermocouple located at the center of the cup. Two different cups were used for complete thermal characterization: plain cups and cups with tellurium and sulfur. In addition to this, inoculated and non inoculated tests were conducted using the plain cups in order to obtain different nodule counts in the melt. For this purpose, approximately 0.20% of a commercial inoculant product (chemical composition: Si = 75-78%, Ca =1.8-2.0%, Zr = 1.3-1.4%, Al = 1.0-1.2% and 0.2-0.5 mm of grain size) was introduced in the corresponding cups before pouring.

After solidification, all metal samples contained in cups were cut and prepared for metallographic inspection. Optical microscopy observations were carried out in the central areas of the samples (where K-type thermocouples are located) in order to estimate nodule counts and then compare them with those predicted using the new computer-aided system based on cooling curves. All the metallographic nodule count values were obtained using a commercial image analysis software.

Apart from thermal studies, experimental tests for evaluating the contraction tendency of alloys were performed using specific cross shaped castings. Chemical bonded sand molds (Figure 6a) were manufactured for this purpose and 0.20% of the commercial inoculant mentioned above was added into them before metal pouring. Resulting cross shaped castings (Figure 6b) had a total volume of 79 cm^3 and were submitted to x-ray inspections in order to detect the shrinkage defects formed into them. The area affected by shrinkage was evaluated from two perpendicular x- ray images analysis, giving values S_1 and S_2 in square centimeters. From these, the volume affected by shrinkage (V_s) was calculated using equation 15 and then compared to the corresponding k factors calculated from the experimental cooling curves.

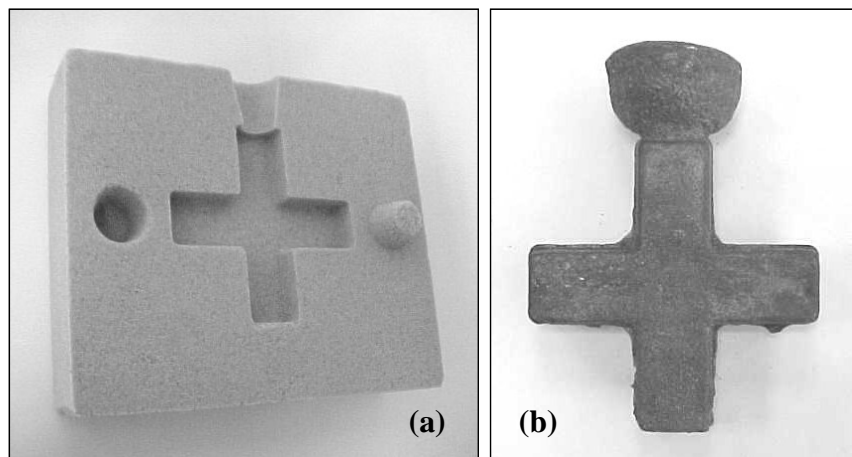$$V_s \ (cm^3) = \frac{S_1 \cdot \sqrt{S_2} + \sqrt{S_1} \cdot S_2}{2}$$

Equation 15

Figure 6. (a) Chemical bonded mold used for shrinkage measuring tests; (b) obtained cross shaped casting.

RESULTS AND DISCUSSION

NODULE COUNT PREDICTION
A nodule count prediction model based on equation 13 has been developed setting up a database which contains all thermal parameters obtained from the experimental cooling curves and the results of the metallographic inspections. In each case, metallographic nodule count estimations were carried out as an average value of three different zones analyzed in the central area (where the thermocouple is located). Carbon, silicon and magnesium contents have been considered as additional fields into the database in order to guarantee the correct formation of graphite nodules. Two different possibilities have been established for determining the chemical composition: the results obtained from spectrometric analysis and its calculation from cooling curves where the metal samples have been treated with tellurium and sulfur. In both cases, similar nodule count predictions are obtained. A free magnesium content of 0.023% has been adopted as the critical limit for obtaining the predicted nodule count values. The effective control of this active element through thermal analysis becomes a very useful tool to minimize the treatment costs and to reduce the influence of high magnesium contents on the shrinkage formation process. If spectrometric Mg content was used for nodule count prediction, a critical value of 0.025% has been adopted for guaranteeing spheroidal graphite formation.

Figure 7 shows a comparative analysis between the nodule count values obtained using equation 13 and the results of metallographic inspections made on all standard samples. A good agreement has been found in all the nodule count range achieved.
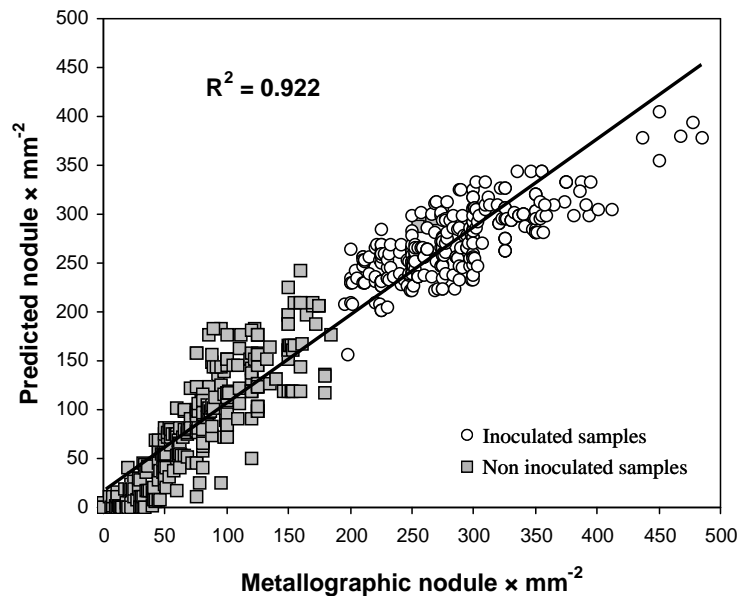

Figure 7. Correlation between predicted N values and metallographic nodule counts for standard TA samples.

Cooling curves recorded from inoculated samples give rise to highest nodule count values (200-450 nodules·mm^{-2}). The lower range was generally achieved in the case of non inoculated metal samples. In this last case, the inoculation effect does not exist and the original nucleation potential of the melts becomes a critical aspect managing the graphite crystallization in the liquid-solid transition.

In order to confirm the validity of the developed predictive model, a comparative study has been made with respect to an extensive amount of real castings, analyzing their nodule count via metallographic inspections. Taking into account that the cooling rate (expressed as the geometric modulus) widely influences the obtained nodule counts, specific areas with similar modulus to the standard samples (0.60-0.65 cm) have been selected in all castings. The cooling curves were simultaneously recorded from poured standard cups in order to obtain the N values in each case. The metal samples used for these thermal characterizations were picked up from the pouring furnaces during each casting manufacturing process.

The results obtained from this study have been plotted in Figure 8. In this figure, data were numbered in the way of a gradual increase in the metallographic nodule count values for a better comprehension. A good correlation can be found between the predicted N values and those obtained from castings inspections. An average error of 3.5% has been obtained for predicted N factor, being the maximum difference of 29 nodules·mm^{-2} for all cases. Although all the castings have been manufactured using inoculated irons, the nucleation capabilities of the metal samples are not similar and nodule counts within the range of 200-310 nodules·mm^{-2} are obtained (Figure 8). This behavior is an effect of different qualities of the melt, which modify the solidification process and the resulting cooling curve shape. As a consequence of this, different N values are finally obtained which agree satisfactorily with the experimental nodule counts.
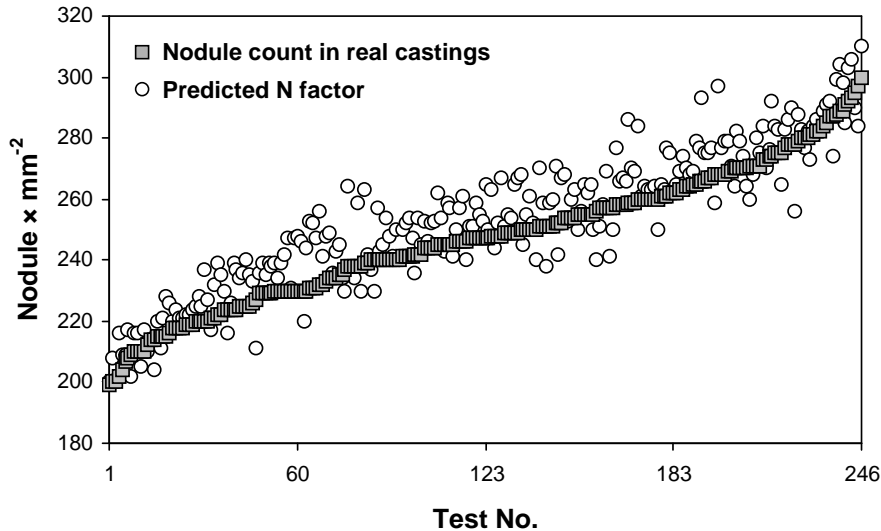
Figure 8. Comparative analysis between the predicted N values and metallographic nodule count values in real castings.

This prediction model only applies to the standard samples used for thermal analysis and those areas with similar geometric moduli in castings. However, it can be used as a useful standard tool in order to quantify the nucleation potential of the melt before pouring, so it can be possible to correct the processing parameters if necessary. Additionally, the prediction of the N factor can be used as an alternative method to metallographic inspections for guaranteeing the correct nodule distribution in manufacturing processes. Further developments are necessary to predict the N factor in different sections of castings taking into account their geometric moduli. This last parameter must be included as a new field into the database and added in expression 13. These studies will be the subject of future works.

MICROSHRINKAGE PROPENSITY ESTIMATION

Shrinkage formation tendency has been evaluated using the k factor directly obtained from the experimental cooling curves. In order to correlate it to the incidence of contraction defects, a new test casting has been designed including a central area prone to this kind of defects. This critical area has a higher geometric modulus (1 cm) than those of surrounding zones and originates a cross shaped distribution (Figure 9). Thus, an isolated mushy area is created during the last steps of the solidification where shrinkage can occur. Simulation studies have been carried out in order to confirm this fact and to obtain the best geometric characteristics for the cross castings. In addition, a standard riser (3.5 cm of diameter, 2.5 cm of height and 0.65 cm of modulus) has been included in the top of the castings to avoid the formation of primary shrinkage defects formed in the early steps of solidification. This feeding system must also promote the appearance of defects only in the central areas (Figure 10).

A total of 210 cross castings (140 inoculated and 70 non inoculated) have been poured in all experimental tests used for setting up the developed database. The obtained cross castings were classified, the defect volumes measured and assigned to the corresponding cooling curves in order to establish a final correlation. Figure 11 shows the results of this study. The highest k factor values are related to the smallest shrinkage volumes (V_s) in the cross castings. Although a progressive reduction of this parameter brings about an important increase of V_s, this tendency is not linear and a maximum volume of 1.5 cm^3 is achieved when k factor is lower than 0.50. This behavior can be considered as a consequence of the maximum contraction capability of ductile irons poured into rigid molds (in this case up to 2% in volume).
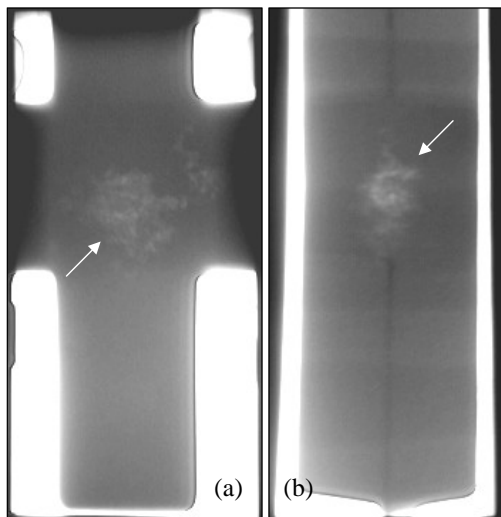
Figure 9. X ray images for shrinkage evaluation: (a) front view and (b) perpendicular view.
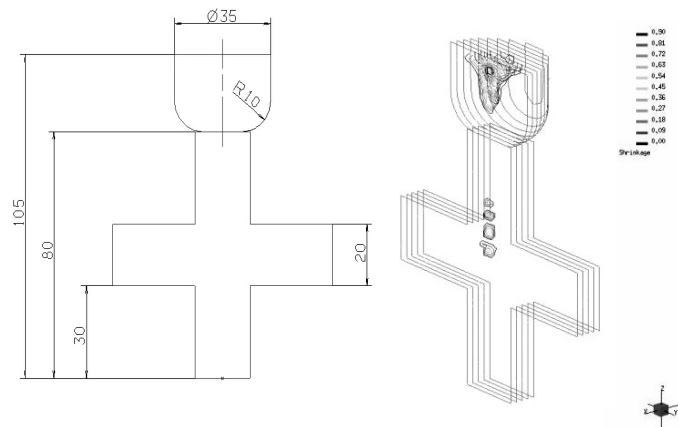
Figure 10. Geometric characteristics of cross castings and shrinkage prediction based on simulation studies.

Although the curves recorded from non inoculated samples usually lead to the lowest k values (0.45-0.75), a few number of these samples with higher eutectic temperatures and melt qualities also give rise to higher k factors (0.80-0.82). In general, inoculation process increases the k values which are then in the range 0.75-0.92. When the solidification of samples with high nucleation potential occurs, metallic contraction due to austenite crystallization can be compensated by the formation of graphite nodules. Thus, smaller contraction periods are obtained in the final steps of the expansion-contraction balance and higher k values are expected. In those cases (that relate to inoculated and several non inoculated samples) the incidence of microshrinkages becomes lower as shown in Figure 11.
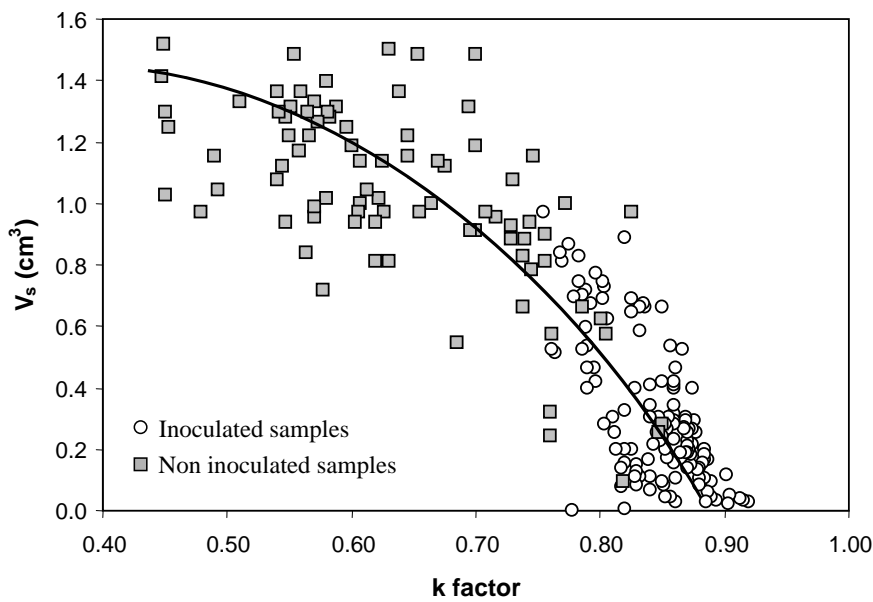
Figure 11. Correlation between the volume of microshrinkage and the k factor.

Metal samples where the nucleation potential is not large show a different solidification process. Under these conditions a decrease of the Te_{min} and an increase of Rc is detected. Comparatively, the crystallization of nodules starts late and is not as favored as in the samples with high nucleation ability. Thus, the resulting austenite-graphite formation balance is not compensated and an important contraction period is found in the final step of the solidification. In this period, dendritic coherency point has been widely exceeded, so the feeding systems are not useful and microshrinkages occur.

In spite of the tendency shown in Figure 11, different microshrinkage volumes have been obtained in cross castings using samples with similar k values. This fact has been assigned to slight differences in the pouring temperature during the cross casting manufacture. In order to evaluate the incidence of the microshrinkage distribution for each k range, all experimental

data have been plotted in Figure 12, expressed as percentage. The analysis of these distributions confirms the correlation observed between the k factor and the size of contraction defects.
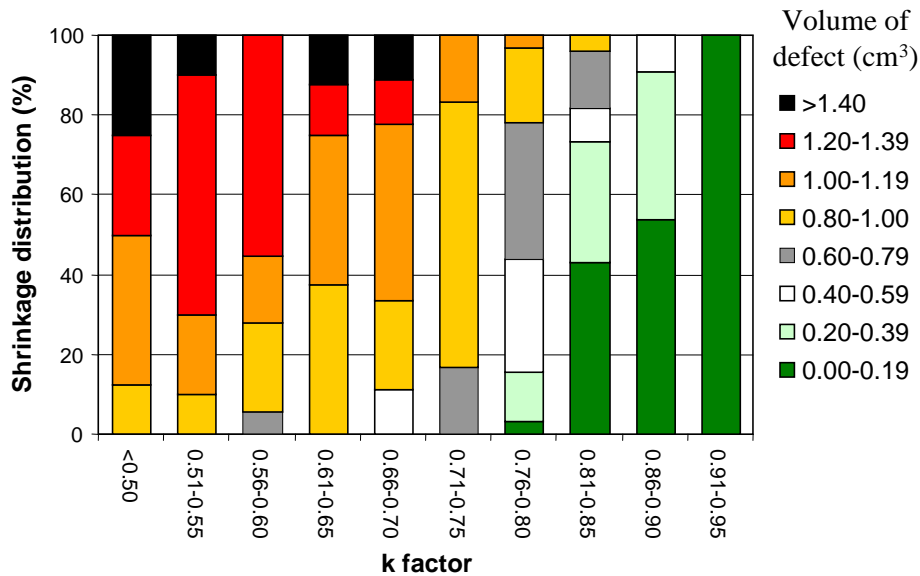

Figure 12. Distribution of microshrinkage size for different k values.

Several tests using real castings have been performed for checking the k factor utility in industrial conditions. The manufacturing process of a specific reference designed for the automotive industry was monitored using thermal analysis and determining the Te_{min}, N and k parameters from the obtained cooling curves. The resulting castings were cut to detect the presence of microshrinkages so as to correlate them to the previous parameters. In order to obtain different melt qualities, green sand molds were poured using inoculated metal samples with similar chemical composition (%C = 3.75-3.80, %Si = 2.40-2.45 and %Mg = 0.030-0.035) and different solidification processes [alloy A: N = 266, k = 0.85, Te_{min} = 1148ºC (2098F) and alloy B: N = 103, k = 0.71, Te_{min} = 1132ºC (2070F)].

Sound castings have only been obtained when alloy A was used. All castings manufactured using Alloy B showed contraction defects as microporosities in the last solidification areas (Figure 13). This results are in good agreement with the correlation found between the k factor and the contraction capability of the melt. Although a correlation between the k factor and the appearance of microshrinkage in specific real castings has been established up to now, a statistical study for the industrial use of this parameter will be made in future works.
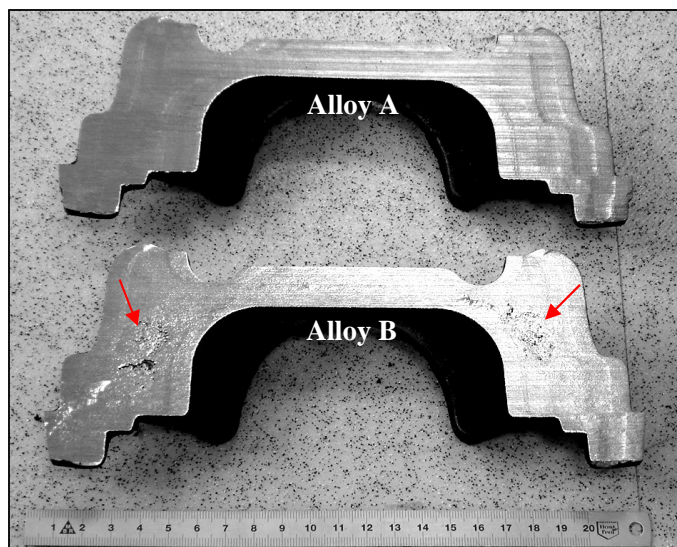

Figure 13. Influence of different melt qualities on the contraction defect appearance.

MELT QUALITY ESTIMATION

The results of the present work indicate that both N and k parameters can be considered as useful indicators for melt quality evaluation in ductile iron manufacturing process. Although an increase of the k factor is often linked to higher predicted nodule counts, the evolution of the k parameter must be only explained on the basis of the contraction-expansion balance in the final step of the solidification. Therefore, it is possible to analyze metal samples with a high nucleation potential and k factors lower than expected. This fact is normally due to the existence of an insufficient graphite expansion at the end of solidification even if the nucleation ability in the liquid state becomes large. Minimum eutectic temperatures also provide information on the solidification patterns and the nucleation potential. Though this parameter is clearly related to the predicted N values, it is not sufficient for quantifying the influence of the subsequent steps of the solidification on the metallurgical behavior of the melt. N and k parameters have been designed for this purpose, showing an appropriate evolution when compared to the experimental behaviors of real castings.

The possibility of gaining adequate knowledge on the different solidification paths in a short time before the pouring process is considered as an important development in order to minimize the appearance of defects in castings. Therefore, melt quality evaluation can be used as a crucial tool to correct or validate in real time the processing parameters. Significant differences among several foundries have been found when adequate melt quality parameters are defined. This is a consequence of different behaviors of metal solidification for each manufacturing process and their own characteristics (pattern plates design, melting methodologies, Mg treatment parameters, inoculation process, molding conditions, etc). These specific factors modify their influence in final metallurgical properties. So it is necessary to carry out a previous study in order to define the more convenient critical values of N and k parameters for a certain foundry.

CONCLUSIONS

According to previous works published in the literature, it has been found that the chemical characteristics of the pouring metal are not the only cause for the different metallurgical behaviors shown in castings. The new system developed in the present work becomes an effective control tool for manufacturing processes in order to guarantee the correct graphite morphology in the solid state and to minimize the shrinkage appearance. Thus, a new solidification model based on experimental cooling curves has been developed for this purpose focusing on two different parameters: predicted nodule count (N) and contraction tendency parameter (k). An extensive number of experimental tests have been made to calculate these parameters and to relate them to the results of metallographic inspections and to the shrinkage incidence in cross shaped castings.

On the basis of this solidification model, a good agreement has been found between the predicted and experimental nodule count values in inoculated and non inoculated standard samples. A further investigation performed with different inoculated quality irons confirms the validity of the obtained correlations. On the other hand, decrease in contraction tendency factors has been related to larger shrinkage volumes in poured cross castings. These results have also been compared and then confirmed by analyzing the contraction defects detected in several real castings manufactured using the same pouring metal in each case. A relationship between both N and k parameters and the nucleation potential of the liquid metal has been found.

Selected parameters become useful for a quick evaluation of the melt quality in industrial conditions before the pouring step. As a consequence of this, it is possible to modify and manage the processing parameters in order to optimize the manufacturing processes. The obtained computer-aided cooling curve analysis can be considered as an inexpensive, simple and fast procedure that finds many applications in the metallurgical and foundry industries. In this case, an important issue is the possibility of combining different studies coming from the melt quality evaluation, the feeding requirements in castings and the resulting mechanical properties.

ACKNOWLEDGMENTS

REFERENCES

1. Li, X., Li, Y., "Evaluation of Melt Quality and Graphite Degradation Prediction in Heavy Section Ductile Iron", *Metallurgical and Materials Transactions*, vol 36A, pp 2455-2460 (2005).
2. Frost, J. M., Stefanescu, D. M., "Melt Quality Assessment of SG Iron Through Computer-Aided Cooling Curve Analysis", *AFS Transactions*, vol 100, pp 189-199 (1992).
3. Sertucha, J., Suárez, R., Legazpi, J., Gacetabeitia, P., "Influence of moulding conditions and mould characteristics on the contraction defects appearance in ductile iron castings", *Revista de Metalurgia. Madrid*, vol 43, pp 188-195 (2007).
4. Li, Y. X., Wang, Q., "Intelligent evaluation of Melt Iron Quality by Pattern Recognition of Thermal Analysis Cooling Curves", *Journal of Materials Processing Technology*, vol 161, pp 430-434 (2005).
5. Li, Y. X., Xu, X. R., Wang, Q., Liu, B. C., "Evaluating Melt Iron Features by Computer Aided Recognition of Thermal Analysis Cooling Curves", *International Journal of Cast Metal Research*, vol 16, pp 41-45 (2003).
6. Skaland, T., "Ductile Iron Shrinkage Control through Graphite Nucleation and Growth", *International Journal of Cast Metal Research*, vol 16, pp 11-16 (2003).
7. Rivera, G. L., Boeri, R. E., Sikora, J. A., "Research Advances in Ductile Iron Solidification", *AFS Transactions*, vol 111, paper 03-159 (2003).
8. Bradley, F. J., Fung, C. A., "Thermal Analysis for Shrinkage Prediction in Commercial Ductile Iron Castings", *Canadian Metallurgical Quarterly*, vol 30, pp 251-260 (1991).
9. Heine, R. W., "Austenite Liquidus, Carbide Eutectic and Undercooling in Process Control of Ductile Base Iron", *AFS Transactions*, vol 103, pp 199-206 (1995).
10. Heine, R. W., "The Fe-C-Si Solidification Diagram for Cast Irons", *AFS Transactions*, vol 94, pp 391-402 (1986).
11. Labrecque, C., Gagné, M., "Interpretation of Cooling Curves of Casting Irons: A Literature Review", *AFS Transactions*, vol 106, pp 83-90 (1998).
12. Sparkman, D., "Understanding Thermal Analysis of Iron", *AFS Transactions*, vol 102, pp 229-233 (1994).
13. Udroiu, A., "The Use of Thermal Analysis for Process Control of Ductile Iron", Proceedings of the Seminarium NovaCast, Camposampiero, Italy (2002).
14. Sillén, R., "ATAS – A Practical Guide for Ductile Iron", NovaCast, internal work.
15. Chen, I-G., Stefanescu, D. M., "Computer-Aided Differential Thermal Analysis of Spheroidal and Compacted Graphite Cast Irons", *AFS Transactions*, vol 92, pp 947-964 (1984).
16. Sertucha, J., Suárez, R., Izaga, J., Hurtado, L. A., Legazpi, J., "Prediction of Solid State Structure Based on Eutectic and Eutectoid Transformation Parameters in Spheroidal Graphite Irons", *International Journal of Cast Metal Research*, vol 19, pp 315-322 (2006).
17. Chang, S., Shangguan, D., Stefanescu, D. M., "Prediction of Microstructural Evolution in SG Cast Iron from Solidification to Room Temperature", *AFS Transactions*, vol 99, pp 531-541 (1991).
18. Barlow, J. O., Stefanescu, D. M., "Computer-Aided Cooling Curve Analysis Revisited", *AFS Transactions*, vol 105, pp 349-354 (1997).
19. Maijer, D., Cockcroft, S. L., Patt, W., "Mathematical Modeling of Microstructural Development in Hypoeutectic Cast Iron", *Metallurgical and Materials Transactions*, vol 30A, pp 2147-2158 (1999).
20. Guo, X., Stefanescu, D. M., "Solid Phase Transformation in Ductile Iron. A Benchmark for Computational Simulation of Microstructure", vol 105, *AFS Transactions*, pp 533-543 (1997).
21. Ribeiro, C., A., S., Santos, D., Baumgart, W., Vilela, F., Henke, C., "New Approach to the Use of Thermal Analysis to Predict Microstructure and Mechanical Properties of As-Cast Ductile Iron", *International Journal of Cast Metal Research*, vol 16, pp 47-52 (2003).
22. Strong, G., R., "Thermal Analysis as a Ductile Iron Molten Metal Processing Evaluation Tool", *AFS Transactions*, vol 91, pp 151-155 (1983).
23. Godsell, B. C., "Preconditioning of Ductile Iron", *AFS Transactions*, vol 78, pp 273-276 (1970).
24. Louvo, A., Pellikka, E. Alhainen, Eklund, P., "Criterion Functions Based on Alloying and Cooling Rate for Simulating the Microstructure and Mechanical Properties of SG Iron Casting", *AFS Transactions*, vol 99, pp 237-244 (1991).
25. Tinoco, J., Delvasto, P., Quintero, O., Fredriksson, H., "Thermal Analysis of Nodular and Lamellar Eutectic Cast Iron under Different Cooling Rates", *International Journal of Cast Metal Research*, vol 16, pp 53-58 (2003).
26. Ekpoom, U., Heine, R. W., "Thermal Analysis by Differential Heat Analysis (DHA) of Cast Iron", *AFS Transactions*, vol 89, pp 27-38 (1981).
27. Ohnaka, I., Iwane, J., Yasuda, H. Zhu, J., "Prediction of Porosity Defect in Spheroidal Graphite Iron Castings", *International Journal of Cast Metal Research*, vol 16, pp 293-299 (2003).
28. Sillén, R., "Production of Ductile Iron Castings in Green Sand Moulds without Feeders", Proceedings of 67th World Foundry Congress, Harrogate, UK, paper 217 (2006).
29. Larrañaga, P., Sertucha, J., Suárez, R., "Analysis of the Solidification Process of Ductile Iron", *Revista de Metalurgia. Madrid*, vol 42, pp 244-255 (2006).

30. Onsoien, M., I., Grong, O, Skaland, T., Jorgensen, K., "Mechanism of Graphite Formation in Ductile Iron Containing Rare Earth Metals", *Materials Science and Technology*, vol 15, pp 253-259 (1999).
31. Fras, E., Wiencek, K., Górny, M. and López, H. F., "Nodule Count in Ductile Iron: Theoretical Model Based on Weibull Statistics", *International Journal of Cast Metal Research*, vol 18, pp 156-162 (2005).
32. Zhao, H., Liu, B., "Simulation of Microstructure Formation of Spheroidal Graphite Iron Casting", *International Journal of Cast Metal Research*, vol 16, pp 281-286 (2003).
33. Dioszegi, A., Svensson, I. L., "Inverse Kinetic Analysis Method to Study Eutectic Growth", *International Journal of Cast Metal Research*, vol 18, pp 41-45 (2005).
34. Emadi, D., Whiting, L. V., Nafisi, S., Ghomashchi, R., "Applications of Thermal Analysis in Quality Control of Solidification Processes", *Journal of Thermal Analysis and Calorimetry*, vol 81, pp 235-241 (2005).
35. Li, Y. X., Hu, X., Xu, X. R., "Pattern Recognition of Thermal Analysis Cooling Curves and Quality Evaluation of Melt Cast Iron", *Journal of Materials Science & Technology*, vol 17, pp 73-74 (2001).
36. Stefanescu, D. M., Qiu, H. Q., Chen, C. H. "Effects of Selected Metal and Mold Variables on Dispersed Shrinkage in SG Cast Iron", *AFS Transactions*, vol 57, pp 189-197 (1995).
37. Suárez, R., "Calidad metalúrgica del hierro. Análisis térmico", Proceedings of 1st Symposium: Azterlan and the Foundry Sector, Bilbao, Spain (2002).
38. Gutiérrez, J. M., "Thermolan, The Metallurgical Prediction Tool", 1st ed., Azterlan, Durango (2005).
39. Sabau, A. S., "Prediction of Alloy Shrinkage Factors for the Investment Casting Process", *AFS Transactions*, vol 114, paper 06-004 (2006).